



**HAL**  
open science

## Nacre-like composites with a soft thermoplastic elastomer matrix

Lucas Rajinthan, Simon Fritz, Igor Galkov, Liuyin Jiang, Sylvain Fournier, Julien Bernard, Sylvain Meille, Aurélien Doitrand, Guilhem P. Baeza

► **To cite this version:**

Lucas Rajinthan, Simon Fritz, Igor Galkov, Liuyin Jiang, Sylvain Fournier, et al.. Nacre-like composites with a soft thermoplastic elastomer matrix. *Composites Science and Technology*, In press, pp.110302. 10.1016/j.compscitech.2023.110302 . hal-04242282

**HAL Id: hal-04242282**

**<https://hal.science/hal-04242282>**

Submitted on 14 Oct 2023

**HAL** is a multi-disciplinary open access archive for the deposit and dissemination of scientific research documents, whether they are published or not. The documents may come from teaching and research institutions in France or abroad, or from public or private research centers.

L'archive ouverte pluridisciplinaire **HAL**, est destinée au dépôt et à la diffusion de documents scientifiques de niveau recherche, publiés ou non, émanant des établissements d'enseignement et de recherche français ou étrangers, des laboratoires publics ou privés.

# Highlights

## **Nacre-Like Composites with a Soft Thermoplastic Elastomer Matrix**

Lucas Rajinthan, Simon Fritz, Igor Galkov, Liuyin Jiang, Sylvain Fournier, Julien Bernard, Sylvain Meille, Aurélien Doitrand, Guilhem P. Baeza

- Simple processing route for Nacre-like composites with a soft thermoplastic elastomer matrix.
- Straightforward manufacturing of gradient microstructures, no specimen size limitation.
- Induction heating can be used to stimulate healing with 3 vol.% of iron nanoparticles.
- Innovative coupling of NMR and DSC enables to probe the polymer state within the composites.

# Nacre-Like Composites with a Soft Thermoplastic Elastomer Matrix

Lucas Rajinthan<sup>a,b</sup>, Simon Fritz<sup>a</sup>, Igor Galkov<sup>a,b</sup>, Liuyin Jiang<sup>a,b</sup>, Sylvain Fournier<sup>a</sup>, Julien Bernard<sup>b</sup>, Sylvain Meille<sup>a</sup>, Aurélien Doitrand<sup>a</sup>, Guilhem P. Baeza<sup>a</sup>

<sup>a</sup>*Univ Lyon, INSA Lyon, Université Claude Bernard Lyon 1, CNRS, MATEIS, UMR 5510, 69621, Villeurbanne, France*

<sup>b</sup>*Univ Lyon, INSA Lyon, Université Claude Bernard Lyon 1, CNRS, IMP, UMR 5223, 69621 Villeurbanne, France, 69621, Villeurbanne, France*

---

## Abstract

We produce nacre-like composites made of a soft thermoplastic elastomer matrix reinforced by alumina platelets, as a flexible and healable alternative to stiff brick-and-mortar materials while keeping their characteristic anisotropic microstructure. Materials are manufactured using step-wise deposition and subsequent controlled evaporation of a suspension containing the polymer and the platelets. Well-aligned microstructures loaded from 15 to 65 vol.% in alumina are obtained through hot-pressing densification of the resulting composites. Remarkably, by combining calorimetry and low-field nuclear magnetic resonance techniques, we emphasize that the polymer mobility decreases significantly in spite of a lower degree of crystallinity when the platelet content is increased. This result sheds light on the origin of the limited quality of samples above 45 vol.%, opening new research directions to improve the design of organic nacre-like composites. Tensile, bending and indentation tests on samples containing up to 45 vol.% in platelets are then used to rationalize the mechanical properties variation related to the polymer state. Finally, we show that the addition of 3 vol.% of Fe nanoparticles into the composites is enough to enable their induction heating that we aim to utilize in the future as a contactless healing method.

*Keywords:* Bio-inspired, Nacre, Alumina platelets, Composites, Thermoplastic polymer, Magnetic hyperthermia

---

---

*Email address:* aurelien.doitrand@insa-lyon.fr, guilhem.baeza@insa-lyon.fr (Guilhem P. Baeza)

## 1. Introduction

Natural nacre presents the noteworthy property to exhibit a non-brittle mechanical behavior although being composed of 95 vol.% of brittle constituent ( $\text{CaCO}_3$ ) [1, 2, 3]. This is mainly due to its defect-free, perfectly stacked, brick-and-mortar structure, made of  $0.5\ \mu\text{m}$  thick  $\text{CaCO}_3$  platelets embedded in 5 vol.% proteins that act as a few nanometers thick interphase. Inspired by the outstanding mechanical behavior reached by nacre in comparison to that of its constituents, tentatives to obtain artificial structures that would reproduce nacre morphology were explored by manufacturing particulate composites consisting of platelets (made of brushite [4], glass [5, 6] or alumina [7, 8]) and of a secondary phase of varying nature (*e.g.* metal [9, 10, 11], glass [8, 12], polymer [13, 14, 15, 16, 17, 18, 19, 20]). An overview of artificial nacre-like materials was provided by Bouville [21].

Several manufacturing processes of full-ceramic nacre-like have been developed so far [21], such as for instance ice templating [22, 23], laser engraving [24], spray forming [5], coextrusion [25] or 3D printing [26]. These processes are generally complex, time-consuming, and limited to small-size specimens, with a typical thickness that does not exceed a few millimeters, with the exception of magnetic assisted slip casting [21] and uniaxial pressing [8, 27]. On the other hand, nacre-like materials made of alumina platelet reinforced polymers are mainly obtained using either Layer-By-Layer (LBL) deposition [28, 29] or preform infiltration [30, 31, 32, 33, 34].

The biggest drawback of LBL deposition is its slow fabrication rate resulting in films that are usually limited to a thickness of ca.  $20\ \mu\text{m}$ . Besides, the infiltration of a preform by polymers is made difficult (if not impossible) because of their high viscosity and requires therefore most often in-situ polymerization of pre-infiltrated monomers. This process can be utilized to prepare either thermoplastic-, rubber- or thermoset-based composites [15] but is not necessarily adapted to complex molecular architectures such as multiblock copolymers, widely used as thermoplastic elastomers (TPE) in the industry. In their comprehensive study, Niebel *et al.* [15] manufactured nacre-like infiltrated ceramic scaffolds using three polymers of very different mechanical properties including PMMA (glass), PUA-PHEMA (cross-linked resin) or PLMA (very soft rubber) in order to evaluate the influence of the polymer phase on nacre-like mechanical behavior. However, none of these three polymers combined a thermoplastic character and flexibility at room temperature, two key ingredients for the design of flexible and healable composites. In addition, the Young's modulus of these three polymers was respectively 2 GPa, 350 MPa and 70 kPa, relatively far from the usual value of "structural" rubbers close to 1-50 MPa.

Yet, a few tentatives of artificial nacre manufacturing relying on a TPE matrix have been proposed. Bonderer *et al.* [35] prepared thermoplastic polyurethane (TPU) reinforced alumina platelet composites by using a combined gel-casting and hot pressing process. They manufactured pore-free composites up to 30 vol.% of alumina platelet. Above this threshold, a dramatic loss of mechanical properties was observed in spite of a growing hard phase content. The presence of pores that possibly initiated cracks in the material was given as an explanation for this phenomenon without however providing systematic characterization nor solution to avoid this deleterious effect.

The purpose of this work is the manufacturing and the investigation of the structure-properties relationship of nacre-like materials based on alumina platelets and a thermoplastic elastomer matrix. Beyond providing flexibility and toughness to our composites, the soft matrix is used in view of a long-term goal, which is to endow these materials with stimulus-healing capabilities. Targeted applications regard any kind of reusable protective equipment such as helmets and knee pads as well as vehicle bumpers. In the present paper, we first describe our processing route that is derived from the LBL philosophy in Section 2. This method is preferred because it enables the production of relatively thick ( $> 1$  mm) and homogeneous sample while making formulation gradient easily accessible. After controlling the porosity and the degree of alignment of the platelets, we focus our attention on the polymer phase and show its influence on the mechanical properties of the composites in Section 3. We finally discuss these results and present preliminary tests regarding stimulus-healing through magnetic hyperthermia in Section 4.

## 2. Materials and Methods

### 2.1. Materials preparation

The polymer matrix consists of a commercial thermoplastic polyurethane (TPU, Desmopan 786-E) purchased from Covestro, Germany. Its glass transition temperature ( $T_g$ ) and its melting point ( $T_m$ ) are respectively ca.  $-30^\circ\text{C}$  and  $150^\circ\text{C}$ . Its density and average molecular weight are respectively  $1.15\text{ g/cm}^3$  and  $188\text{ kg mol}^{-1}$ . The alumina platelets characterized by a thickness of ca. 500 nm and a mean diameter of ca.  $10\text{ }\mu\text{m}$  are RonaFlair-White Sapphire from Merck, Germany. THF was used to mix intimately the TPU and the platelets. The whole processing route is described in Figure 1.

Appropriate amounts of TPU and platelets were weighted and incorporated within THF so that the total solid content was approximately 80 wt.%. The mixture was then stirred at  $40^\circ\text{C}$  during 12 hours in a round-bottom flask to ensure the total TPU dissolution and poured layer-by-layer in a PTFE-coated glass mold. The mixture was tentatively casted over 1-, 5- or 20- cycle(s). Single-layer

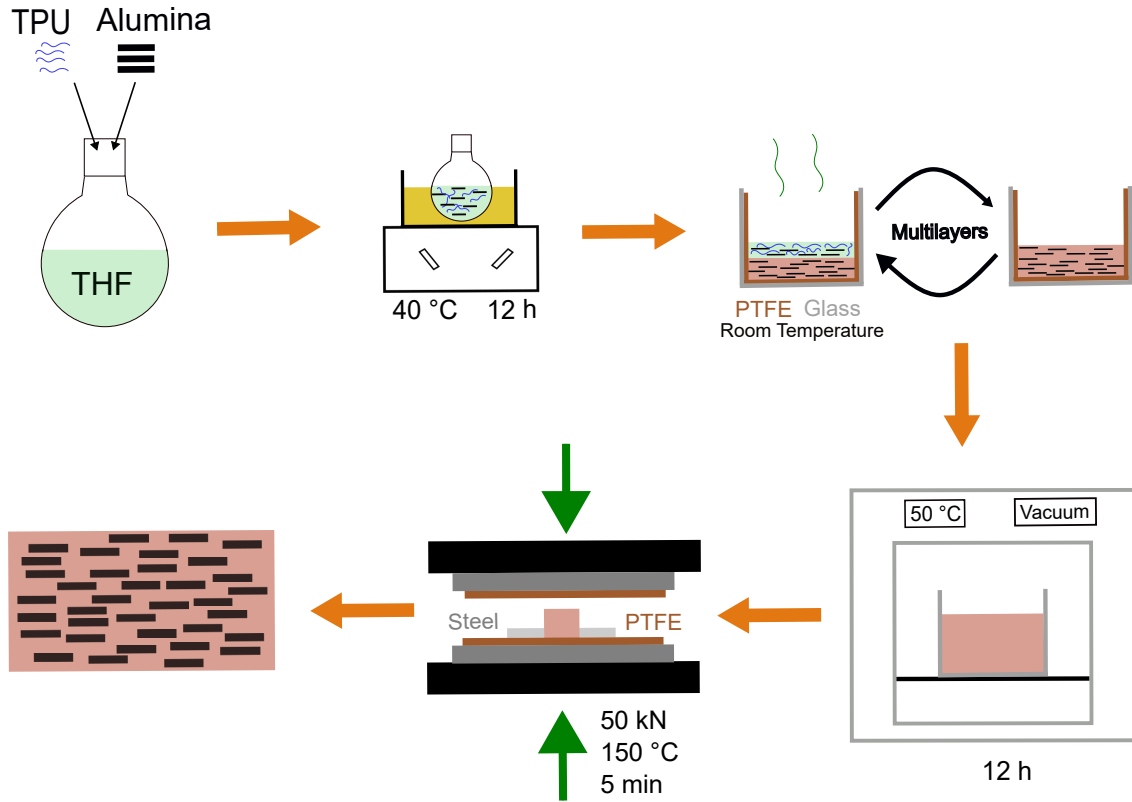


Figure 1: Nacre-like composites processing consisting of step-wise casting of a TPU-platelets fillers dispersion and subsequent hot-pressing.

addition yielded platelet volume fraction differences up to 20 wt.% between the specimen top and bottom. This effect was reduced to a few percents by using 5- or 20- layer additions, resulting in a homogeneous platelets dispersion. The 20-layer addition was consequently adopted in this work. Casting cycles were performed every 20 min under a fume hood at room temperature so that each layer had time to gelify partly. This gelification allows to limit massive sedimentation of the platelets while letting the inter-layer diffusion of the TPU chains. In other words, it ensures a homogeneous filler dispersion and maximize the material cohesion. At the end of the casting procedure, the sample is dried under a fume hood overnight to remove most of the residual solvent and subsequently vacuum dried at 50 °C for 12 hours. Finally, the samples are hot-pressed at 0.5 bar - 150 °C ( $\approx T_m$ ) for 5 min and gently cooled down under pressure in 10 min to room temperature. Series of thermogravimetry experiments under argon were performed on samples extracted from various sample's locations and on both sides, providing a platelet content uncertainty of  $\pm 2$  vol.%. At last, we obtained disk-shaped specimen of typical diameter and thickness of 5 cm and 1 mm respectively.

## 2.2. Methods

### 2.2.1. Scanning Electron Microscopy (SEM)

Composite micrographs were obtained using a VEGA3 from TESCAN (USA). Imaging was performed using a secondary electron detector and 10 kV acceleration voltage. To improve the quality of SEM observation, the composites were subjected to ion milling (ILION II 697, GATAN) for 2 hours. Samples were stuck onto a titanium mask (GATAN) and milled with two Ar ion beams with a tension acceleration of 6 keV before being covered with a thin layer of gold. This method provided us with polished area of ca.  $10 \times 100 \mu\text{m}^2$  enabling clear distinction between the polymer matrix and alumina platelets.

### 2.2.2. Shore Hardness

Hardness was measured using a 3114 Shore D tester (ZwickRoell, France) on both top and bottom of samples in order to evaluate their homogeneity through the sample thickness. Measurements were repeated five times on both sides of the samples.

### 2.2.3. Porosimetry

Archimede's method: the density was measured on a minimum of 3 locations with a density kit (Mettler Toledo, USA) and ethanol (96 wt.%) as a solvent. Although results showed a progressive growth of the porosity up to 5 % in the composite containing 35 vol.% in platelets, the method was judged to be insufficiently accurate at higher alumina content so we completed it with image analysis. Image processing and analysis : SEM 2D observations of ion-polished samples were analyzed using Fiji. The pore surface fraction was calculated based on a gray level threshold of the image on at least  $500 \mu\text{m}^2$  areas. For each platelet volume fraction, the pore surface fraction was estimated based on at least 3 zones. In addition, OrientationJ Fiji plug-in [36] was used to determine the platelet orientation based on image structure tensor calculation using a local averaging window.

### 2.2.4. Differential scanning calorimetry (DSC)

Differential scanning calorimetry (DSC) analyses were performed on a TA Instruments Q10 calorimeter under  $50 \text{ mL min}^{-1}$  nitrogen flow. Temperature and enthalpy calibrations were performed using indium and zinc standards. DSC capsules containing about 10 mg of composites were heated from room temperature up to  $220^\circ\text{C}$  and kept isothermally for 5 min before being cooled down to  $-70^\circ\text{C}$  and kept isothermally for 5 min followed by a second heating up to  $220^\circ\text{C}$  at a heating rate of  $5^\circ\text{C min}^{-1}$ . Data presented in this work correspond to the second heating step.

### 2.2.5. Low-Field Nuclear Magnetic Resonance (LF-NMR)

LF-NMR Free Induction Decay (FID) measurements were performed on a Bruker Minispec mq20, at a 20 MHz proton resonance frequency. The samples were placed in 1 cm diameter tubes and their height was fixed to  $(2.0 \pm 0.5)$  mm. The temperature was controlled using a BVT 3000 heater. Prior to each measurement, the temperature was stabilized for 10 min. The signal at short time was systematically set between 60 and 100% of relative intensity by adjusting the gain of the spectrometer and limited to 200  $\mu$ s acquisition time to avoid any magnetic field inhomogeneity.

### 2.2.6. Tensile test

Uniaxial tensile tests were performed at room temperature at a constant strain rate of 5 mm min<sup>-1</sup> on a tensile test machine 1/ME (MTS, USA) equipped with either 1 kN or 10 kN load cell for the composites and the neat TPU respectively. The samples were shaped into dumbbell pieces of effective dimensions  $20 \times 5 \times 2$  mm<sup>3</sup>. Pieces of rubber were glued to the pure TPU samples in order to avoid any slip issues. A minimum of three tests was performed for each platelet volume fraction configuration.

### 2.2.7. Three points bending test

Three-points bending tests were carried out on plain samples using uniaxial testing machine (Instron 8562, High Wycombe, UK) with 18 mm support span distance. The thickness and width of the samples were respectively  $(5.0 \pm 0.2)$  mm and  $(3.0 \pm 0.1)$  mm. Tests were displacement controlled at a crosshead speed of 0.5 mm min<sup>-1</sup>. The platelet main alignment plane normal corresponded to the specimen thickness direction, *i.e.* to material testing in 'across direction' [2].

### 2.2.8. Stiffness determination

The material Young's modulus  $E$  was estimated as the slope at the origin of stress-strain curves. Because the material consisted of a platelet reinforced elastomer, nonlinear stress-strain curves were obtained. For each sample, a linear regression of the stress-strain curve was performed including both a linear (providing  $E$ ) and a quadratic term active from a given fixed strain threshold  $\varepsilon_0$  (providing the constant  $\xi$ ), which writes:

$$\hat{\sigma} = E\varepsilon + \xi \langle \varepsilon - \varepsilon_0 \rangle_+^2, \quad (1)$$

where  $\langle \cdot \rangle_+$  are Macaulay brackets and  $\varepsilon_0$  is determined as the strain  $\varepsilon$  which minimizes the difference between  $\hat{\sigma}$  and the stress measured experimentally.

### 2.2.9. Instrumented indentation test

Indentation tests were performed at room temperature using an Electroforce 3200 machine (BOSE, USA) having a 1 mm diameter Tungsten Carbide spherical tip at a load-controlled speed in the range 0.20 to 0.30 N s<sup>-1</sup>. The displacement of the tip was measured using a capacitive sensor with a 0.1 μm resolution and the load with a 22 N cell.

### 2.2.10. Rheology

Measurements were all performed using 8 mm diameter parallel plates in a strain-controlled rheometer (ARES 2kFRTN1) with convection oven allowing a temperature control better than ±1 °C. Frequency sweep experiments were performed at 180 °C to melt crystallites and enhance chain mobility, ensuring a reasonably fast flow of the material, providing similar conditions as during the healing procedure. The strain amplitude was progressively decreased from 10 % for neat TPU down to 5 %, 3 %, 1 %, 0.3 % and 0.1 % for composites loaded with 5 vol %, 10 vol %, 15 vol %, 20 vol % and 30 vol % of alumina platelets respectively. All the materials were loaded with 3 vol.% of Fe nanoparticles, which corresponds to the formulation required to perform stimulus healing.

## 3. Results and discussion

### 3.1. Platelets alignment and porosity

Once the processing route completed, the sample quality is estimated through two criteria that are 1) the alignment of the platelets with respect to the plane orthogonal to the uniaxial pressure direction, *i.e.* along the specimen thickness direction, and 2) the porosity content. Optimizing and reducing respectively these criteria is expected to enhance both the mechanical and barrier properties of the manufactured samples. Note that micro-computed tomography observations of the manufactured materials does not enable to quantify the platelets alignment due to a too low resolution. Platelet alignment was therefore quantified based on SEM observations.

In Figure 2, we quantify the orientation of platelets in a sample containing 55 vol.% in alumina by means of image processing. A color code is provided in Figure 2a to facilitate the visualization of the orientation distribution around the average angle value that is set to 0°. Our processing route is found to yield samples characterized by a full-width at half maximum of  $\Delta\theta=25.6^\circ \pm 16^\circ$  (Figures 2b-c), which is considered to be satisfying given its simplicity. In fact, Saad *et al.* [8] reported a full width at half maximum of about 20° in their fully inorganic materials processed by hot-pressing. Also, Bonderer *et al.* obtained quite similar values in their platelets reinforced TPU ( $14^\circ < \Delta\theta < 26^\circ$ )[35] and

polypropylene ( $10^\circ < \Delta\theta < 25^\circ$ ) [37] processed by a combination of gel-casting and hot-pressing. Interestingly, while  $\Delta\theta$  was observed to grow monotonically with the platelet content in the latter works, Figure 2c rather suggests a constant alignment distribution in our case. It is however important to remind the reader that significantly better alignment of the platelets ( $\Delta\theta < 8^\circ$ ) could be achieved by functionalizing their surface and using advanced air-water interfacial processing, as demonstrated in the earlier works of Bonderer *et al.* [28, 29].

Beyond quantifying the platelet alignment in the composites, image processing is further used to evaluate their porosity, in complement to Archimede's method. The results are presented in Figure

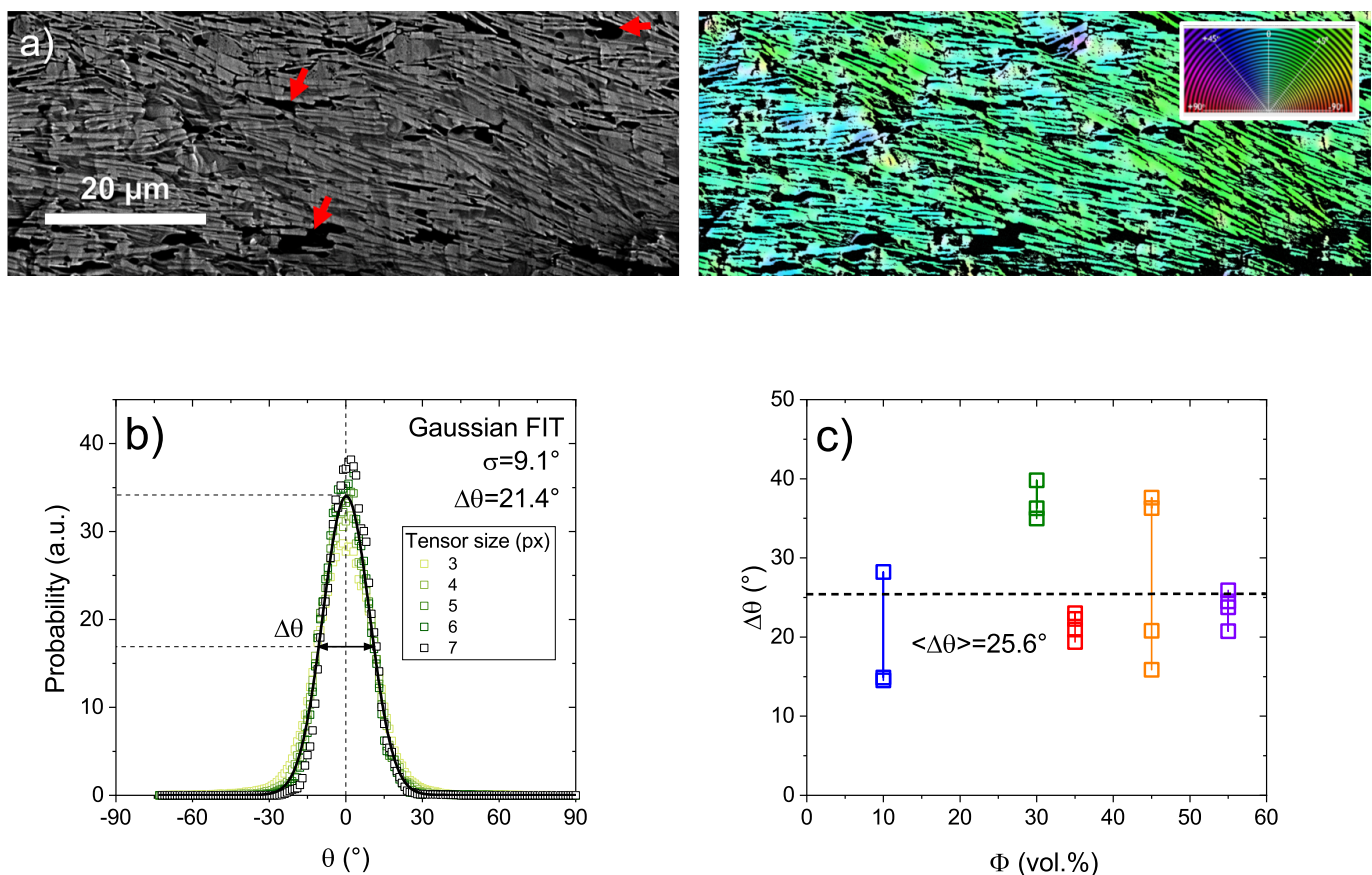


Figure 2: Distribution of the orientation of platelets in a composite loaded with 55 vol.% in platelets. a) SEM-BSE micrograph (left) and its colored version (right) based on the orientation-color code displayed at the top-right corner. Red arrows emphasize the presence of pores (detected above 40 vol.%, see text). b) Alignment of the platelets for various tensor sizes used for the image treatment highlighting the robustness of the method,  $\Phi = 55$  vol.%. Full width at half maximum is denoted  $\Delta\theta$ . The solid line is a concatenated Gaussian fit in which the average is fixed to  $\bar{\theta} = 0^\circ$  resulting in a standard deviation of  $\sigma = 9.1^\circ$  corresponding to  $\Delta\theta = 21.4^\circ$ . c)  $\Delta\theta$  as a function of the platelet content. The dashed line represents the average value calculated from all the samples

3 revealing a strong increase of the porosity content for  $\Phi > 45$  vol.%, reaching up to 12 % for  $\Phi = 65$  vol.%.

In addition and despite scattered results, Archimede's method was systematically found to provide values in the 0-5 % interval for  $\Phi > 45$  vol.%, confirming qualitatively the image analyses. In contrast, no porosity was detected for  $\Phi \leq 35$  vol. %.

Shore-D experiments were also used as a simple probe of the materials quality as presented in the inset of Figure 3a. For a given platelet volume fraction, hardness relative variations at different sample locations are smaller than 3%, which highlights the homogeneity of the microstructure within a sample. These variations slightly increase for the specimens having the highest platelet volume fraction. Besides, whatever the platelet volume fraction, average hardness differences between the sample top and bottom surfaces are smaller than 5 %, which evidences similar microstructure and properties on the top and the bottom of the casted samples in spite of the gravity-driven nature of our processing route. Beyond evidencing a relative homogeneity in the microstructure and resulting mechanical properties, these tests also reveal a decrease in the hardness from  $\Phi > 45$  vol.%. Such lower mechanical properties upon adding alumina platelets are undoubtedly related to the presence of

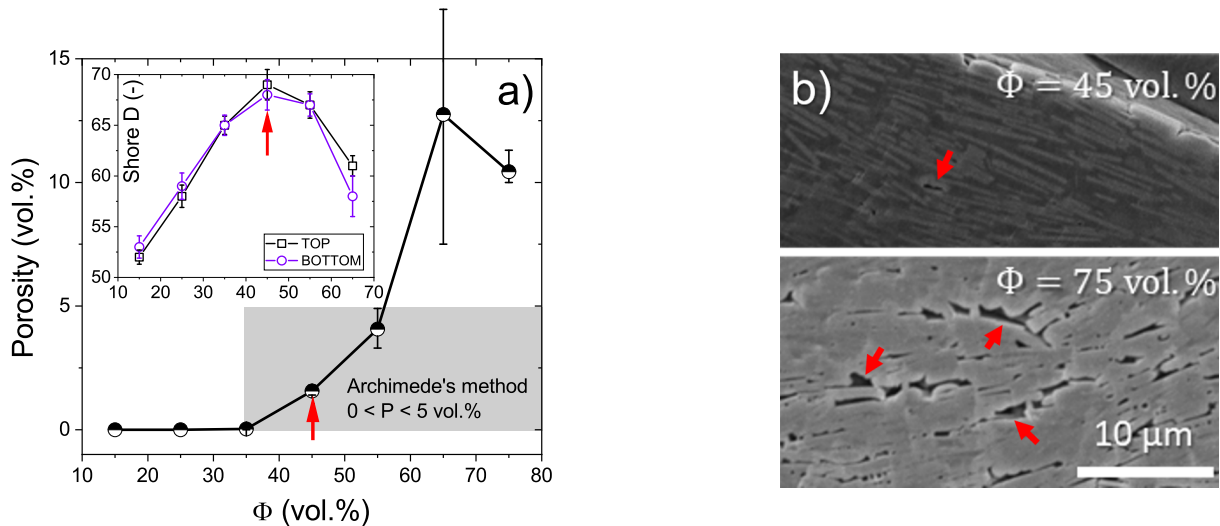


Figure 3: a) Porosity as a function of the platelet content estimated through image analysis. The grey zone corresponds to the porosity estimated through Archimede's method leading to erratic values all comprised in the 0-5 vol.% interval for platelet volume fractions above 35 vol.%. Inset: Shore D hardness as a function of the platelet volume fraction. Error bars indicate the standard deviation (5 measurements on each side). Red arrows highlight the correspondence between the upturn of the porosity and the maximum in terms of hardness. b) SEM micrographs highlighting the presence of pores in samples loaded with more than 40 vol.% in platelets. Top (BSE detector): 45 vol.% (limited defects). Bottom (SE detector): 75 vol.% (massive defects). Arrows emphasize the largest defects in both cases.

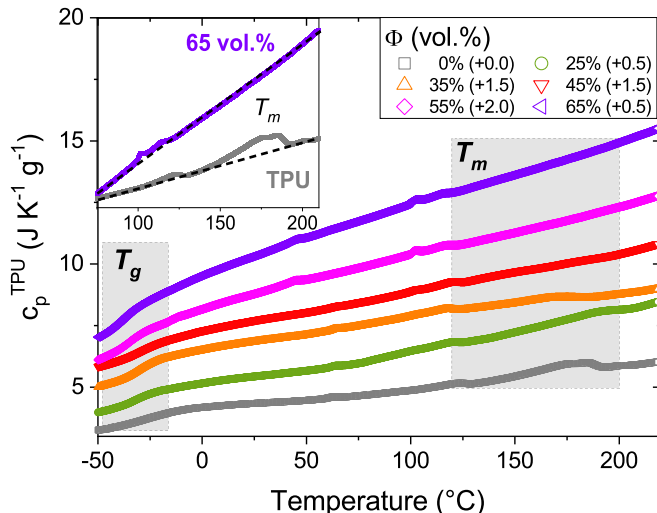


Figure 4: Specific heat capacity of the TPU embedded into the composites loaded with 25, 35, 45, 55 and 65 vol.% in platelets and the corresponding neat TPU matrix. Data are vertically shifted for the sake of clarity (see caption). Grey zones highlight the glass transition  $T_g$  and the melting temperature  $T_m$  ranges. Inset: Zoom-in the TPU and the 65 vol.% data highlighting the difference of melting profile. Data were matched at low temperature for the sake of clarity. Dashed lines represent basis lines.

defects in the samples that one can put in parallel with the growing porosity content (see red arrows in Figure 3). In the next section we shall rationalize the limitations of our processing route in terms of platelet content by investigating the state of the polymer matrix embedded into the composite.

### 3.2. Characterization of the Embedded Matrix

In order to understand the limits of our processing route and to rationalize the mechanical properties of the composites, we focus on the state of the polymer embedded into the composites. We remind the reader that the TPU is a semi-crystalline multiblock copolymer that contains ca. 6 wt.% of crystallites that mainly melt in-between 150 °C and 200 °C when the polymer is casted alone (see Figure 4). The flexibility of the TPU is provided by its soft segments characterized by a glass transition temperature of ca.  $-30$  °C. The incorporation of alumina platelets into the TPU thus results in a triphasic composite made of 1) soft organic domains, 2) organic crystallites and 3) 2D inorganic fillers of much higher rigidity. The thermal characteristics of the neat TPU can be extracted from differential scanning calorimetry (DSC) experiments, as illustrated in Figure 4 where we present the specific heat capacity of the TPU as a function of the temperature for several inorganic filler volume fractions. Apart from revealing thermal transitions, DSC temperature ramps further enable to precisely measure the specific heat capacity of the material, passing expectedly from ca.  $2.5$  to  $6$   $\text{J K}^{-1} \text{g}^{-1}$

from  $-50\text{ }^{\circ}\text{C}$  to  $220\text{ }^{\circ}\text{C}$ . This technique is also convenient to probe the state of the polymer embedded into composites where the heat capacity of the polymer phase can be extracted according to

$$c_p^{\text{TPU}} = \frac{C_{\text{Comp}} - C_{\text{filler}}}{m_{\text{TPU}}} = \frac{C_{\text{Comp}} - c_p^{\text{filler}} m_{\text{filler}}}{m_{\text{TPU}}}, \quad (2)$$

as proposed by Holt *et al.* [38]. In this expression,  $C_{\text{Comp}}$ ,  $C_{\text{filler}}$ ,  $c_p^{\text{filler}}$ ,  $m_{\text{filler}}$  and  $m_{\text{TPU}}$  are respectively the heat capacity of the composite, the heat capacity of the filler, the specific heat capacity of the filler, the mass of filler within the measured sample and the corresponding mass of TPU. Because in our case  $c_p^{\text{filler}} \approx 0.7\text{ J K}^{-1}\text{ g}^{-1}$  (alumina) and since its temperature dependence is weaker than the TPU one, we approximate  $c_p^{\text{TPU}}$  based on the second term of Eq. (2) with  $C_{\text{filler}}$  being constant on the whole temperature range. The resulting  $c_p^{\text{TPU}}$  in presence of fillers are plotted in Figure 4 and vertically shifted for the sake of clarity. Interestingly, while the glass transition temperature of the soft-segments, taken as the  $c_p$  inflexion point at low temperature in Figure 4, is not significantly influenced by the filler volume fraction in the composites (ranging erratically from  $-35\text{ }^{\circ}\text{C}$  to  $-25\text{ }^{\circ}\text{C}$  for filler volume fractions between 0 and 65 vol.%), a major effect is observed at higher temperature. In fact, the variations of  $c_p^{\text{TPU}}$  around the melting point of the neat TPU seem to be almost eliminated, indicating an important loss of crystallinity ( $X_c$ ). This effect is further emphasized in the inset of Figure 4 where the signals of the neat TPU and of the composite containing 65 vol.% in platelets are compared and confronted to linear variations. In addition to the influence on the TPU crystallization, it also appears that the temperature dependence of the  $c_p^{\text{TPU}}$  is stronger for high platelet volume fractions, particularly above  $\Phi=45\text{ vol.}\%$ . While the precise origin of this phenomenon remains unclear to us, we believe that it may be caused by the (heat consuming) desorption of the TPU hard-segments from the platelet polar surface.

In order to deepen the characterization of the TPU within the composites and particularly address the question of the chain adsorption onto ceramic platelets, we conducted systematic low-field NMR experiments. In particular, we measured the FID of composites containing 15, 25, 35, 45, 55 and 65 vol.% in platelets from room temperature (ca.  $40\text{ }^{\circ}\text{C}$ ) up to the hot-pressing temperature ( $160\text{ }^{\circ}\text{C}$ ). This method first consists of placing the sample in a permanent magnetic field to align all the hydrogen spins in the same direction ( $Oz$ ) before flipping them in the orthogonal plane ( $Oxy$ ) using a radiofrequency wave ( $\pi/2$  pulse). The LF-NMR spectrometer then measures the decreasing magnetization of the sample as a function of time (precession) enabling to discriminate different dynamical responses, characteristic of different phases. FID experiments have been used successfully to quantify the fraction of adsorbed chains and their dynamical slowing down. [39, 40].

In Figure 5, we present FID normalized signals measured on a composite containing 25 vol.% in

platelets at temperatures ranging from 40 °C up to 160 °C. As expected, increasing the temperature results in flattening the signal corresponding to longer H-atoms transverse relaxation time (denoted  $T_2$  in the literature), synonymous of a higher mobility of the organic phase. These results are systematically fitted by using a 2 components Kohlrausch-Williams-Watts (KWW) function (Eq. (3)) with the aim to extract two populations of polymer segments: 1) rigid (or constrained) and 2) soft (or mobile). Note that even in the case of the neat TPU, two modes are required to fit the data appropriately owing to the presence of highly rigid crystalline domains.

$$I_{xy}(t) = I_1 \exp\left[\left(\frac{-t}{\tau_1}\right)^{\beta_1}\right] + I_2 \exp\left[\left(\frac{-t}{\tau_2}\right)^{\beta_2}\right]. \quad (3)$$

In this expression  $I_1$  and  $I_2$  are the amplitudes of the two modes being respectively proportional to the number of constrained and mobile H-atoms;  $\tau_1$  and  $\tau_2$  are the transverse relaxation times of the hard and soft populations;  $\beta_1$  and  $\beta_2$  are the corresponding parameters describing the broadness of the relaxation modes. The latter values are systematically found to be slightly lower than 1, which indicates a stretched-exponential profile as it is generally the case in these experiments. A direct quantitative comparison of the experiments is made possible through signal normalization:

$$I_n(t) = \frac{I_{xy}(t)}{I_1 + I_2}, \quad (4)$$

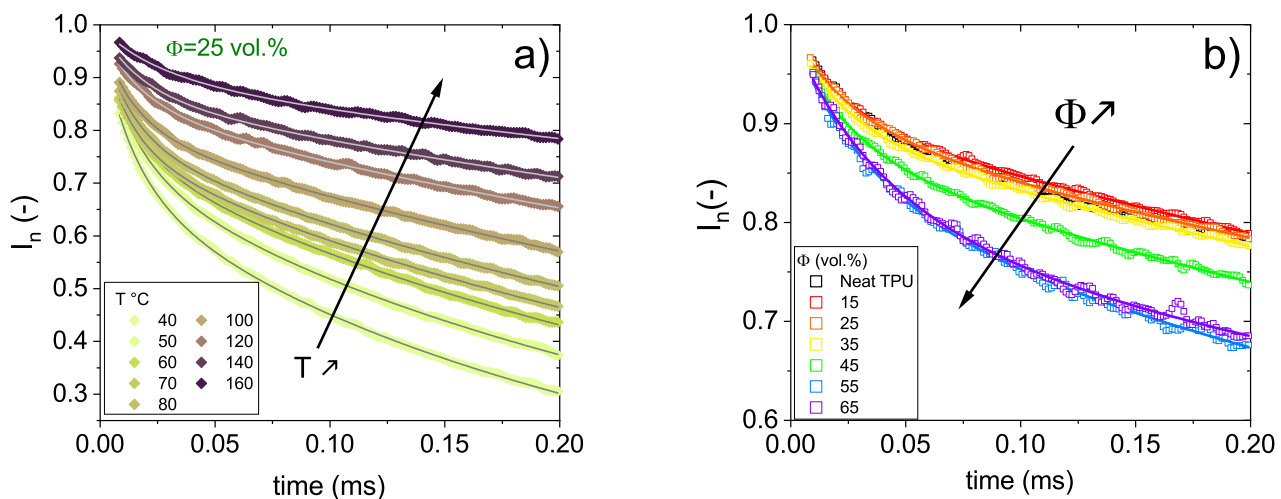


Figure 5: a) Free Induction Decay normalized intensity as a function of the experimental time for the composite loaded with 25 vol.% in platelet from 40 °C to 160 °C. Solid lines are fit based on Eq. (3) b) Analog signals for composites loaded with 15, 25 and 35 vol.% as well as the neat TPU matrix measured at 160 °C.

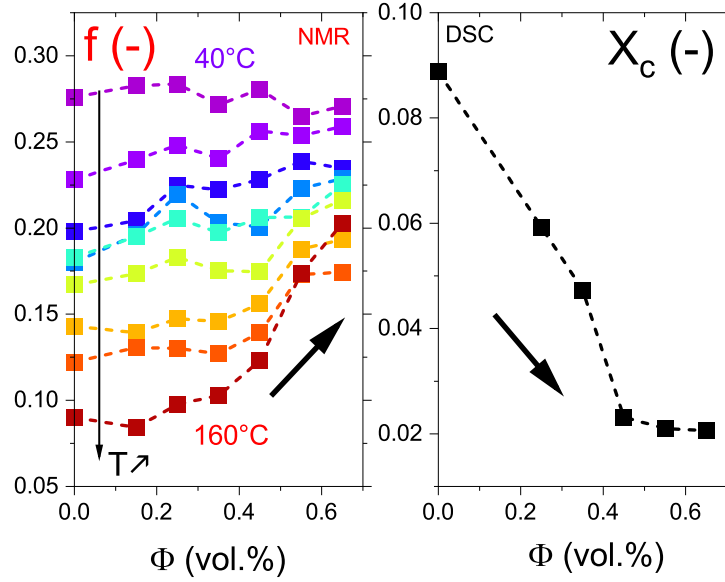


Figure 6: (Left) Fraction of rigid polymer measured by LF-NMR in composites loaded from 15 vol.% to 65 vol.% as well as the neat TPU matrix between 40°C and 160°C. (Right) Mass fraction of crystallites within the TPU phase measured by DSC as a function of the volume fraction in platelets in corresponding composites 160 °C.

and the fraction of rigid segment within the organic phase writes

$$f = \frac{I_1}{I_1 + I_2}. \quad (5)$$

While the effect of the temperature is somewhat expected, we present in Figure 5b the variation of  $I_n$  as a function of time for different platelet contents at 160 °C. Interestingly, the intensities are first seen to overlap from 15 vol.% to 35 vol.% before decreasing significantly from 45 vol.% and above. Since the temperature corresponds roughly to the temperature used for the hot-pressing step, this result indicates that the chain mobility during the processing route is significantly reduced for composites loaded with more than 45 vol.%. In fact, although the relaxation time of the rigid phase does not evolve significantly with the platelet content,  $\tau_1 = 2.70 \pm 1.55$  ms (in agreement with quite similar  $T_g$  in Figure 4), we show in Figure 6 that the fraction of rigid segments grows from ca. 6 % to 21 % when passing from the neat TPU to the 65 vol.% composite. This "rigidification" upon increasing the platelet content is also observed at lower temperatures at which the difference between hard and soft phase dynamics is less pronounced.

We also report in Figure 6 the evolution of the crystallites content in the TPU as a function of the platelet content. This parameter is extracted according to

$$X_c = \frac{\Delta H}{\Delta H^*}, \quad (6)$$

where  $\Delta H$  and  $\Delta H^*$  are respectively the specific melting enthalpy of the TPU accessible through the DSC experiments presented in Figure 4 and the corresponding value for a hypothetical fully crystalline material being  $138 \text{ J g}^{-1}$  assuming our polymer is similar to the one studied by Griffiths *et al.* [41, 42]. In contrast with the growing fraction of rigid polymer detected by LF-NMR, the significant decrease of  $X_c$  with increasing the platelet content unambiguously indicates that the TPU becomes progressively unable to crystallize. This phenomenon is well-known in semi-crystalline polymer based nanocomposites and arises from the steric hinderance caused by the nanoparticles as well as favorable interactions between the polymer and the filler surface (see e.g., silica reinforced PEO [43]). The emphasis of these two opposite trends is particularly relevant to rationalize both the limitations in terms of processing route and the mechanical properties presented in section 3.3. We develop this point in the discussion presented in section 4.

### 3.3. Mechanical Properties

In this section we characterize the mechanical properties of presumably viable composites (*i.e.*, defect-free and non-porous samples) by means of tensile, bending and indentation experiments.

In Figure 7a, we present engineering stress-strain curves obtained through quasi-static tensile solicitation for the neat TPU and composites loaded with 15, 25 and 35 vol.% in platelets, three specimens were tested for each platelet volume fraction. These tests highlight a strong influence of the platelet volume fraction on the mechanical properties of the composites. They first emphasize a pronounced enhancement of the Young's modulus ( $E$ ), from ca. 17 MPa to 1 GPa, and of the yield stress ( $\sigma_y^t$ ) from ca. 4 MPa to 16 MPa.  $\sigma_y^t$  is defined as the stress corresponding to the crossover of linear fits performed at low strain and in the strain hardening regime for the neat TPU and the 15 vol.% composite and to the stress maximum ( $\varepsilon < 1$ ) for the 25 vol.% and 35 vol.% composites. Conversely, the strain at "first" failure ( $\varepsilon_{\max}$ ), corresponding to the first drop of stress, and the toughness ( $K$ ), quantified by the area under the stress-strain curve decrease importantly, passing respectively from 10.3 down to 0.4 and from  $150 \text{ mJ mm}^{-3}$  down to  $5 \text{ mJ mm}^{-3}$  for the neat TPU and the 35 vol.% composites respectively. In addition, the strain hardening character observed in the neat TPU is seen to progressively disappear in the composites when increasing the platelet content. Such a behavior can be rationalized based on the loss of mobility of the polymer phase (see NMR experiments), favoring delamination events rather than conformation changes (stretching) responsible of the strain hardening. In Figure 7b, we focus our attention on the way the samples behave after they reach  $\varepsilon_{\max}$ . In particular, we show that when  $\Phi = 25 \text{ vol.}\%$  (or  $\Phi = 15 \text{ vol.}\%$  - not reported here), the composite fails in a step-wise manner, contrarily to samples loaded with either 0 or 35 vol.% that

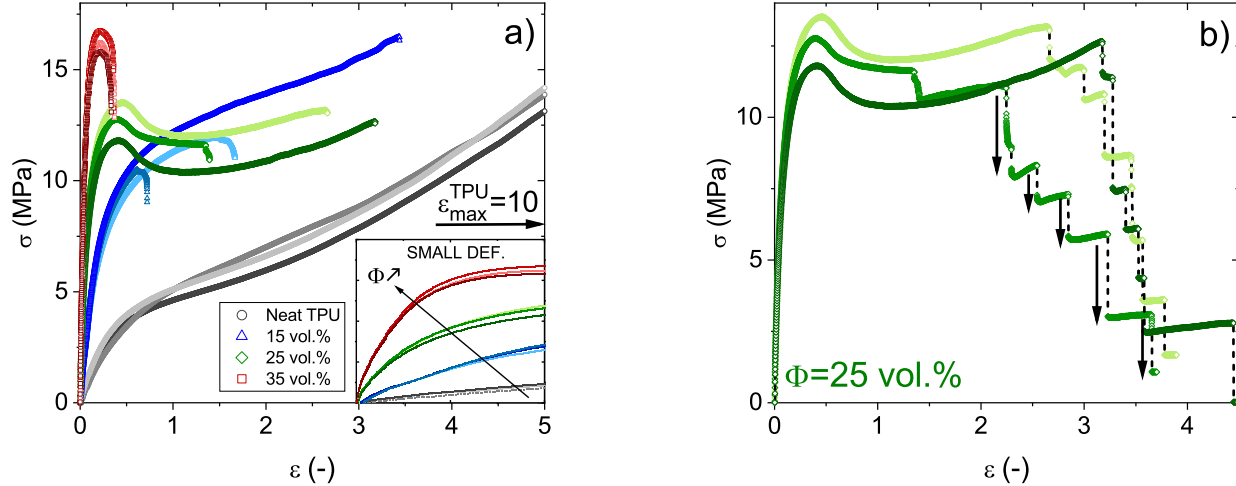


Figure 7: a) Tensile stress as a function of strain for composites loaded with 15, 25 and 35 vol.% as well as the Neat TPU matrix. Inset: Zoom-in at low deformation. The TPU fails around  $\varepsilon = \varepsilon_{max}^{TPU} = 10$ . Data are stopped right after the "first failure" event, *i.e.*, the first significant stress drop. b) Full tensile tests highlighting the step-wise failure of composites loaded with 25 vol.% in platelets.

breaks suddenly, regardless of their brittle or ductile character. In fact, the results presented in Figure 7b systematically show that the failure occurs through 5-7 steps strongly suggesting the successive failure of (single and/or groups of) layers with increasing deformation. Post-mortem observations revealing decohesion and various failure events actually confirmed this hypothesis.

It is worth noting that the timescale relevant for the segmental relaxation (responsible for the glass transition) at room temperature is smaller than a microsecond, which means that at low deformations, there is no reason to expect a significant influence of the strain rate on the mechanical properties. For what concerns high deformations, increasing the strain rate is expected to enhance the strain hardening in the nonlinear regime and possibly cause a premature failure of the material [44, 45].

To improve the knowledge of the structural properties of these composites, the mechanical characterization must be extended to other testing configurations. Following this idea, we present in Figure 8 bending characterizations of samples containing 15, 25, 35 and 45 vol.% in platelets. In this case, the neat TPU is too flexible to be measured appropriately with our testing equipment. For each formulation, three tests are reported and the area they define is colored to highlight the variability on the mechanical behavior due to the manufacturing process and the platelet volume fraction. As expected, the addition of platelets is seen to strongly increase the stiffness at low displacement that is related to the Young's modulus, which is estimated to pass from  $121 \text{ MPa} \pm 14 \text{ MPa}$  at 15 vol.%

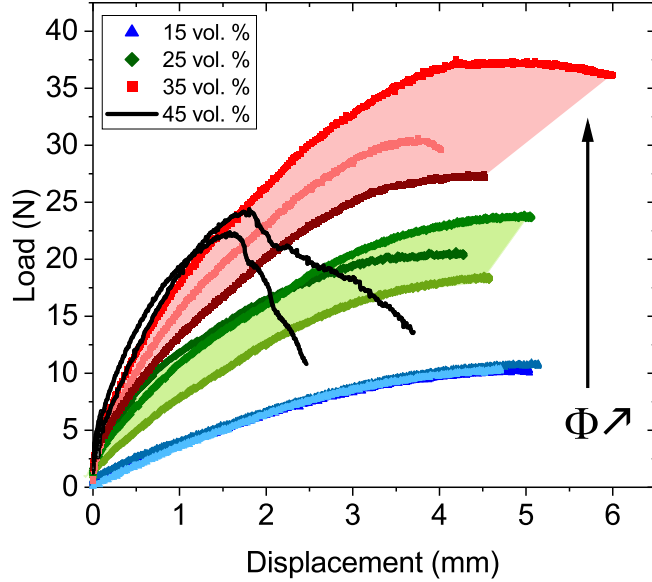


Figure 8: Bending force as a function of the displacement for composites loaded with 15, 25, 35 and 45 vol.% in platelets. The neat TPU matrix was too flexible to be measured in the same conditions.

to  $775 \text{ MPa} \pm 127 \text{ MPa}$  at 45 vol.% (see Supporting Information section 1). Conjointly, the average stress at failure ( $\sigma_f^b$ ) increases from 10 MPa to 32 MPa between 15 vol.% and 35 vol.% in platelets before falling to ca. 23 MPa at 45 vol.% as one may have anticipated from Figure 3, indicating that 2-3 % of pores is enough to dramatically influence the mechanical properties at high deformation. It is further noteworthy that the deflection (and thus the strain) at maximum stress in truly non-porous samples ( $\Phi \leq 35 \text{ vol.}\%$ ) remains constant, about 5 mm. Beyond intrinsic composites properties, one can also remark that the scattering of the force-displacement curves increases with the platelet content suggesting the growing presence of micro-heterogeneities in highly reinforced materials.

Finally, we present in Figure 9 instrumented indentation tests serving to characterize the resistance to local penetration of our composites. While these experiments have been repeated at various penetration rates and different locations showing no significant impact (see Supporting Information section 2), we focus on the data recorded at  $0.2\text{-}0.3 \text{ N s}^{-1}$  for samples loaded with 10, 20 and 30 vol.% in platelets as well as the neat TPU. As clearly noted in Figure 9, a full recovery of the penetration depth is observed after unloading, with no trace left on the samples surface whatever the platelet volume fraction. As one may have anticipated based on the growing Young's modulus detected in both tensile and bending tests, the load required to penetrate the composites, and thus the hardness,

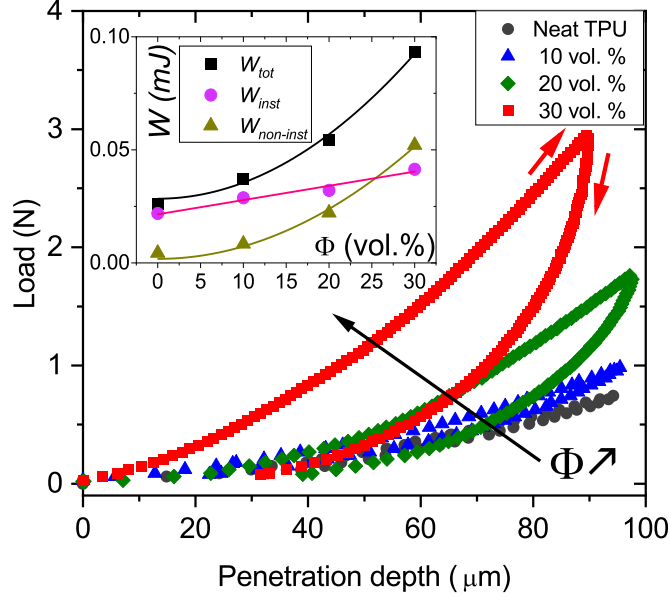


Figure 9: Indentation force as a function of the penetration depth for composites containing 10, 20 and 30 vol.% in platelets and the corresponding neat TPU matrix. Inset: Total, reversible and irreversible work as a function of the platelet volume fraction. Solid lines are fit to the data with  $\Phi^2$  dependence ( $W_{\text{tot}}$  and  $W_{\text{non-inst}}$ ) and  $\Phi$  dependence ( $W_{\text{inst}}$ ).

strongly increases with increasing platelet content. This trend is observed from both the upper and the lower curves corresponding respectively to the loading and unloading steps. Hardness and Young's modulus are not the most relevant parameters to be extracted from this series of tests, due to the pronounced non-linear behavior, coupled with the strong recovery after unloading, and a energy-based approach seems preferable to analyze the data. By analyzing each experiment, one can then extract characteristic parameters enabling to rationalize the experiments from an energetic point of view:

- $W_{\text{tot}}$ , the "total" work required to penetrate the sample (surface under the upper - loading - curve)
- $W_{\text{inst}}$ , the "instantaneous" work stored by the sample and released upon unloading (surface under the lower - unloading - curve)
- $W_{\text{non-inst}}$ , the "non-instantaneous" work dissipated within the sample (surface in-between upper and lower curves).

The variation of these parameters as a function of the platelet volume fraction is presented in Figure 9 inset. In addition to the above-mentioned growth of  $W_{\text{tot}}$  with increasing  $\Phi$ , it clearly appears that

its derivative progressively increases too, being compatible with a  $\Phi^2$  dependence (black line). The same trend is observed for  $W_{\text{non-inst}}$  (brownish curve - triangle markers), indicating a quickly growing number of dissipative events. In contrast,  $W_{\text{inst}}$  follows a linear trend characterized by a moderate slope (purple line).

## 4. Discussion

### 4.1. On the structure-mechanics relationship

Our "easy" process enables manufacturing alumina platelet reinforced elastomers with a large range of platelet volume fractions ( $\Phi \leq 75$  vol.%) and no limitation on the specimen thickness. It yields composites exhibiting a main platelet alignment plane, with local disorientation  $\Delta\theta=14-40^\circ$  for  $\Phi$  varying from 10 vol.% to 55 vol.%. Of a particular interest, no porosity is detected for materials satisfying  $\Phi \leq 40$  vol.% making them probably viable for engineering applications. In this range, a higher platelet content results in an increase of the material Young's modulus, yield strength, hardness and contact energy dissipation in return of a toughness decrease as measured in tension. Because the Young's modulus and the yield stress can respectively be improved up to 60 and 4 times with respect to the neat TPU matrix, a large range of mechanical behavior (and possibly barrier properties) is accessible. Conversely, the pore content is observed to grow from 2 % to 13 % for  $\Phi$  increasing from 45 vol.% to 75 vol.%, which results in brittle materials that cannot be used for structural applications. We demonstrate that this transition can be rationalized by investigating the polymer phase, as discussed in the next section.

Interestingly, similar observations on the mechanical properties were made by Bonderer *et al.* [35] for a quite similar alumina platelet reinforced thermoplastic polyurethane, albeit made of a softer polymer. No particular investigations regarding the pore content nor the polymer state were nevertheless provided. The direct comparison of our composites and those manufactured in [35] is displayed in Tables 1 and 2 respectively, where the relative variation of the Young's modulus, maximum stress and strain as well as the area under the stress-strain tensile curves ("toughness") for various platelet contents are reported. The graphical representation of these Tables are provided in Supporting Information section 3.

A brief glance at these tables is enough to realize that both studies are comparable, making a global interpretation more relevant. The main conclusions are as follows :

- The Young's modulus of the composite can be enhanced by a factor higher than 50 with respect to the matrix for ca. 40 vol.% in platelets. It seems nevertheless that the reinforcement of

$\Phi$ (vol.%)	$E/E^{TPU}$	$\sigma_{max}/\sigma_{max}^{TPU}$	$\varepsilon_{max}/\varepsilon_{max}^{TPU}$	$K/K^{TPU}$
15	8.1	0.465	0.323	0.226
25	40.2	0.458	0.389	0.256
35	59.9	0.572	0.038	0.034

Table 1: Our matrix properties :  $E^{TPU} = 16.9$  MPa ;  $\sigma_{max}^{TPU} = 28.4$  MPa ;  $\varepsilon_{max}^{TPU} = 1030$  % ;  $K^{TPU} = 150.9$  mJ/mm<sup>3</sup>

$\Phi$ (vol.%)	$E'/E^{TPU'}$	$\sigma'_{max}/\sigma_{max}^{TPU'}$	$\varepsilon'_{max}/\varepsilon_{max}^{TPU'}$	$K'/K^{TPU'}$
11	3.4	0.532	0.560	0.574
22	9.3	0.386	0.155	0.162
33	19.8	0.439	0.085	0.112
43	33.6	0.395	0.020	0.021
53	106	0.207	0.07	0.003
63	12.5	0.120	0.02	0.006
73	7.3	0.043	0.01	-

Table 2: Bonderer's matrix properties :  $E^{TPU'} = 4.6$  MPa ;  $\sigma_{max}^{TPU'} = 41.2$  MPa ;  $\varepsilon_{max}^{TPU'} = 1910$  % ;  $K^{TPU'} = 244.1$  mJ/mm<sup>3</sup>

the material is significantly higher in our case for intermediate platelet volume fractions. This difference is likely caused by the slightly different chemical nature of the polymers used in both works. Further increase of the platelet content is however detrimental because of the apparition of defects as confirmed by porosity and hardness analyses in Figure 3.

- Between 20 vol.% and 40 vol.%, the composite toughness strongly decreases by a factor of ca. 7-20 with respect to the neat TPU. It is interesting to remark that Bonderer *et al.* [35] reported significantly higher relative toughness at 11 vol.% than us at 15 vol.%. In fact, this platelet volume fraction range usually represents a properties turn in nanocomposites because of the percolation of slowed down polymer layers located at the interface with the reinforcing fillers [46, 47].
- At 40 vol.%, the composite exhibits a maximum in terms of average stress at failure due to enhanced stiffness whereas it almost breaks in a brittle way close to  $\varepsilon = 5$  %, in agreement with the above-mentioned drastic decrease in toughness. This recalls the wide range of mechanical behavior, from a soft elastomer to a strong composite, easily accessible with our process.

Focusing on toughness aspects, it appears that, under bending and even more evidently under indentation loading, increasing  $\Phi$  enhances energy dissipation contrary to what is observed under tensile loading. The contact energy dissipation is for instance multiplied by 4 when passing from the neat TPU to the composite loaded with 30 vol.% in platelets, while keeping the capability to recover its initial shape after a certain time. These composites, loaded with 10-30 vol.% seem thus promising candidates to target applications requiring energy dissipation due to contact or impact while being stiffer and harder than pure TPU. Indentation testing is representative of contact loading, involving mainly compressive stresses, *i.e.* without crack propagation. The early fracture noted in tensile tests on composites due to the presence of rigid platelets and to the limited deformability of the polymer does not impact the behavior in indentation. On the contrary, the presence of platelets increases the amount of stored energy in the composites. Under bending loading, samples are able to deflect without fracture, illustrating the limited influence of early fracturation observed in tensile tests.

#### 4.2. How the polymer state inform us on the processing route limitations

A main limitation of our processing route is related to manufacturing composites having a high platelet volume fraction, which actually results in poor mechanical behavior due to the presence of defects and pores above 40 vol.%. In this context, one should pay a particular attention to the ability of the polymer to diffuse in-between the platelets during the drying step and to its chemical compatibility (or wettability) with the platelets surface. For example, in a composite having 50 vol.% in platelets and exhibiting a perfectly homogeneous platelet distribution ( $\Delta\theta = 0^\circ$ ), the average inter-platelet distance in the dry state would tend towards the platelet thickness, *i.e.* 500 nm, which should be largely sufficient for the polymer chains to diffuse between the platelets. Indeed, the polymer chain molar mass magnitude lies around  $200 \text{ kg mol}^{-1}$ , which corresponds to an average end-to-end distance of  $\sqrt{\langle R^2 \rangle} = bN^{0.5} \approx 45 \text{ nm}$ , where  $b$  and  $N$  are respectively the Kuhn length (ca. 1 nm) and the number of Kuhn-mer (uncorrelated repetition units, close to 2000). Despite this argument which plays in favor of a possible manufacturing of specimens having platelet volume fractions theoretically higher than 90 vol.%, the analysis presented in previous sections shows that the material hardness, strength and toughness start to decrease from 40 vol.% due to the presence of defects, pores, and polymer-rich zones. The origin of the limited platelets wettability at high  $\Phi$  must then resides within its enthalpic interactions with the polymer. Since the available space between two layers of platelets (ca. 500 nm) is much larger than the size of a molecule (ca. 45 nm end-to-end distance), the polymer confinement does not originate from entropic considerations but is rather due to enthalpic interactions between the chains and the platelets. As a consequence, modifying the TPU molecular weight is not expected

to have a significant influence on the polymer chain confinement between the platelets.

DSC experiments presented in Figure 4 actually highlight favorable interactions between the two constituents through (i) the loss of crystallinity of the TPU, passing from ca. 6 wt % to 0 wt % and (ii), its apparent growth of specific heat capacity, suggesting (heat consuming) desorption events. These results and interpretations are strongly supported by low-field NMR experiments presented in Figure 5 that unambiguously evidence that the polymer rigid fraction (*i.e.*, having a low mobility) strongly increases with increasing  $\Phi$ . Although the exact nature of the physical bond(s) existing between the polymer and the platelets is unknown, we believe that it relies on the affinity of the highly polar polyurethane hard-segments and the hydroxyl groups at the alumina surface, as already observed in similar materials [41]. In consequence, manufacturing materials having higher platelet volume fractions endowed with a defect-free and well-aligned microstructure could possibly be attained by :

- improving the interactions between the platelets and the polymer (wettability) by limiting the number of blocks, *e.g.*, using triblock instead of multiblock copolymers, or increasing the overall chain polarity by choosing another soft-segment chemistry.
- decreasing the polymer molecular weight when increasing platelet volume fraction so as to improve the polymer diffusion between the platelets. This may lead to a loss of material ductility, which is anyway unavoidable when increasing the platelet volume fraction.

#### 4.3. Towards Stimulus Healing: Magnetic responsive Nacre-like composites

Although nacre-like composites are endowed with superior mechanical properties, particularly owing to tortuous crack propagation prior to failure, an important limitation resides in their single-use nature. In what follows, we discuss about a possible healing procedure based on magnetic hyperthermia.

Magnetic hyperthermia is growingly used in material science to heal polymer-based goods in which responsive (nano)particles are incorporated [48]. It consists of irradiating the material with an oscillatory magnetic field of typical frequency (100-1000 kHz) and amplitude (1-20 mT). The particles absorb the radiation and transform it into heat through different mechanisms according to their size and nature [49], favoring the polymer mobility. While millimetric and conductive particles can generate heat through Eddy currents, micrometric and nanometric particles produce heat through magnetic walls motion and Néel relaxation, regardless of their electric conductivity. Heat might also be produced by Brownian relaxation in low-viscosity media and by friction [41, 50]. In this context, the use of nano-magnetite  $\text{Fe}_3\text{O}_4$  or nano-iron Fe is common and has already shown an interest for industrial

applications. Healing through magnetic hyperthermia presents many advantages among which its contactless nature, the possibility to heat selected parts of a material, its low thermal inertia and its tunability that relies on both the stimulus characteristics and the material formulation.

While our long term goal is to manufacture healable nacre-like materials, this ambitious achievement requires two *sine qua non* conditions. First, the material must be reweldable, *i.e.*, it must flow on a reasonable time scale upon heating. Second, both the magnetic field and the material formulation must be adapted so as the temperature can reach (at least) the TPU melting point to promote polymer mobility and diffusion through the cracks. It is important to realize that while increasing the content in responsive nanoparticles will help to reach a higher temperature, it is detrimental for the macroscopic flowing and platelet alignment - the adjustable parameters must then be balanced carefully.

Following this logic, we present preliminary results that support the feasibility of a magnetic hyperthermia healing in Figure 10. In this case, 3 vol.% of polydisperse Fe nano- (and submicro-) particles were added into composites loaded with either 10 or 15 vol.% in platelets; the resulting microstructure is presented in Figure 10a where both Fe particles and alumina platelets are well visible. As presented in Figure 10b, the incorporation of these responsive objects enables to easily

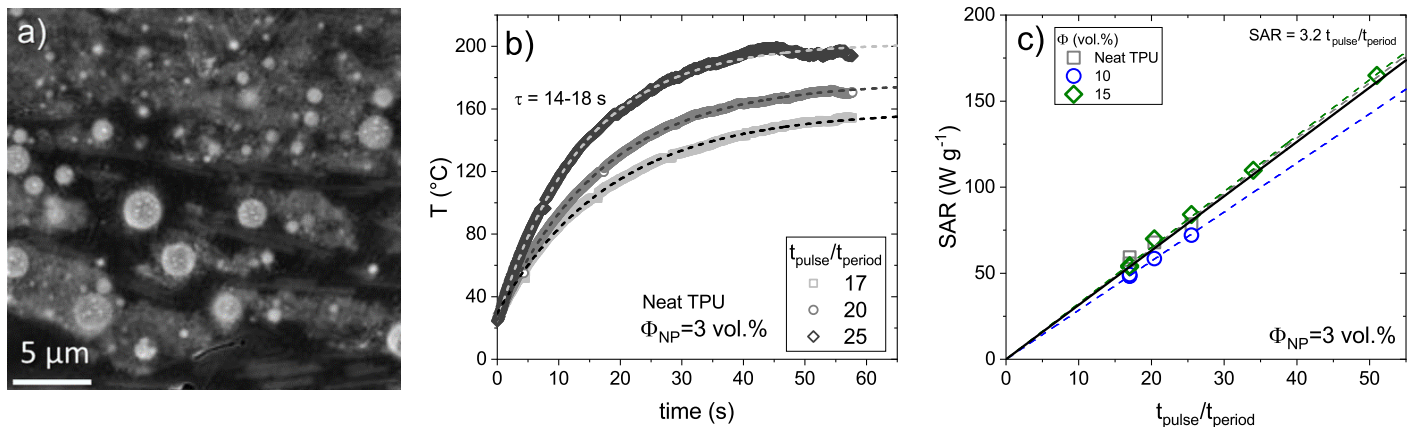


Figure 10: a) SEM micrographs showing the presence of (polydisperse) Fe particles (3 vol.%) together with alumina platelets (15 vol.%) within the TPU matrix. b) Temperature vs. time measured from a neat TPU loaded with 3 vol.% of Fe nanoparticles at various magnetic inductor powers ( $t_{\text{pulse}}/t_{\text{period}}$ ). Dashed lines are fit to the data with the Box-Lucas equation (see text). c) Specific absorption rate vs. magnetic inductor power for neat TPU and composites loaded with 10 and 15 vol.% in platelets. Dashed lines are linear fits corresponding to each sample. The black solid line is a concatenated fit emphasizing the similar magnetic sensitivity of the three samples, all containing 3 vol.% in Fe nanoparticles.

reach temperatures higher than the TPU melting point, with a fine control of the terminal temperature provided by the tunable pulse duration we apply with our device. The ratio  $t_{\text{pulse}}/t_{\text{period}}$  actually represents the time fraction for which the pulsed magnetic field is effectively applied [41]. Interestingly, we remark that the ability of the material to produce heat is not altered by the presence of alumina platelets. In fact, Figure 10c reports the specific absorption rate (SAR), *i.e.*, the specific dissipated heat as a function of  $t_{\text{pulse}}/t_{\text{period}}$ , showing similar behavior for the neat TPU and both composites loaded with 10 and 15 vol.% in platelets. The SAR can be extracted from the  $T(t)$  curves by focusing on data at short time such as

$$SAR = \frac{c_p^{\text{comp}}}{x_{\text{NP}}} \frac{dT}{dt} \Big|_{t \rightarrow 0}, \quad (7)$$

where  $c_p^{\text{comp}}$  is the specific heat capacity of the composite calculated through a mixing rule and  $x_{\text{NP}}$  is the mass fraction of magnetic nanoparticles. Although this result could have been anticipated due to the low-diamagnetic properties of alumina (no shielding effect), its confirmation ensures that similar mechanisms (including possible nanoparticles motion and friction) occur in the whole set of samples.

Lastly, we report in Figure 11 the linear viscoelastic properties of the corresponding materials measured at 180°C. As expected, the neat TPU above its melting point exhibits a loss modulus ( $G''$ ) higher than its storage modulus ( $G'$ ) on the whole frequency range, corresponding to a liquid-like material able to flow in a few seconds in spite of the presence of 3 vol.% of Fe nanoparticles. The situation is qualitatively similar for the composites loaded with 5, 10 and 15 vol.% in platelets although the viscosity is expectedly higher and would therefore require longer healing time to ensure the same level of reparation. The increment of viscosity is nevertheless moderated because of the limited specific surface area of the micronic platelets (ca.  $3.5 \text{ m}^2 \text{ g}^{-1}$ ) and their relatively low volume fraction ( $\Phi \leq 15$  vol.%). At higher platelets contents ( $\Phi = 20$  and  $30$  vol.%),  $G' > G''$  on the whole frequency range being synonymous of the materials gelation, *i.e.*, viscosity divergence, preventing chains diffusion and healing capability. In this case, an additional mechanical action such as hot-pressing will be required to recover the integrity of the material.

## 5. Conclusion

To summarize, we have reported an "easy" layer-by-layer processing route enabling to manufacture nacre-like composites made of a soft thermoplastic elastomer matrix reinforced by alumina platelets. Beyond the homogeneous samples treated in the present work, this method offers the possibility to produce easily composites with a gradient of properties. Although the volume fraction in platelet was varied from 0 up to 75 vol.%, defects free samples could not contain more than 40 vol.% in

inorganic fillers. In the 0-40 vol.% range, the composite could reach Young’s modulus of ca. 60 MPa and tensile yield stress of 16 MPa, corresponding to an enhancement of the TPU properties by a factor ca. 60 and 4 respectively. Tensile tests were completed by performing bending and indentation experiments providing a complete picture of mechanical properties, confirming notably the interest of these materials in contact/shock applications.

The loss of properties above 40 vol.%, already reported in the literature, was rationalized through a combination of calorimetry and nuclear magnetic resonance experiments. While the former revealed a drastic loss of the polymer crystallization upon the addition of platelets, the latter indicated a growingly hindered polymer phase, demonstrating through quantitative arguments that the lack of chain mobility in highly reinforced composite was at the origin of the processing difficulties. This outcome suggests therefore to reduce the molecular weight of the TPU chain and possibly modify the chemical nature of the soft-segment to enhance the platelet-polymer compatibility.

Lastly, we have proposed to use magnetic hyperthermia as a way to heal damaged nacre-like composites by adding a restricted amount (3 vol.%) of responsive nanoparticles (Fe) in the brick-and-mortar structure. Preliminary tests have demonstrated that it was possible to reach temperature

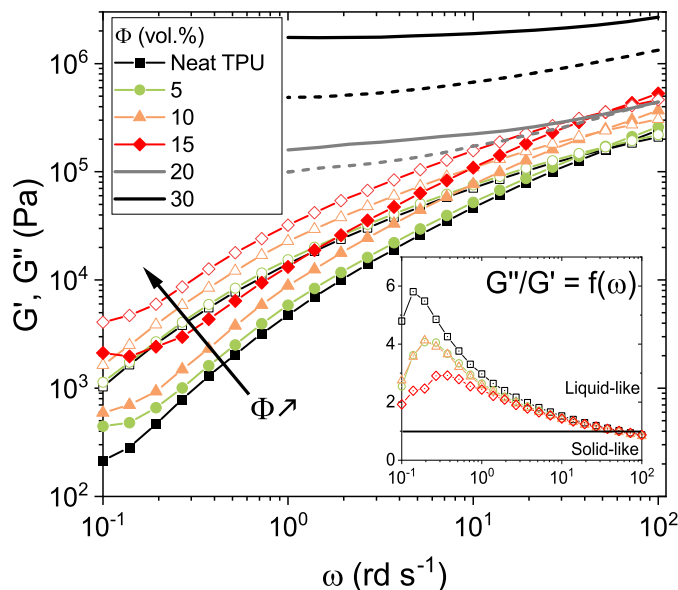


Figure 11: Storage ( $G'$ , plain symbols) and loss ( $G''$ , hollow symbols) shear moduli as a function of the frequency for the neat TPU and responsive composites loaded with 5, 10 and 15 vol.% of platelets. These materials contain 3 vol.% of Fe nanoparticles. Solid and dashed lines respectively represent  $G'$  and  $G''$  for samples loaded with 20 and 30 vol.% in platelets (see caption) but no Fe nanoparticles. Inset: Corresponding loss factor  $G''/G'$  for  $\Phi \leq 15$  vol.% as a function of the frequency highlighting the similar liquid-like behavior.

higher than the polymer melting point in a few seconds regardless of the platelet content in the composite. Materials containing between 10 and 20 vol.% in platelets have been characterized rheologically to evidence their ability to flow macroscopically in a reasonable time scale ensuring efficient healing of damages specimen. Comparison of the pre- and post- damaging mechanical properties is the next step towards the development of this technology and will be treated in a subsequent article. In addition, characterization of the anisotropic material properties will be further studied [8, 51, 52, 53, 54], which is often disregard in the literature about artificial nacre-like materials.

## **6. Acknowledgement**

All the authors thank Bérangère Lesaint, Sandrine Cardinal and Pablo Griffiths (MATEIS, INSA-Lyon) as well as Gildas Coativy (LGEF, INSA-Lyon) and Carlos Fernandez de Alba (IMP, INSA-Lyon) for their technical support and advice regarding some data treatment. The authors also thank Françoise Méchin, Ahmed Belhadj and Vivien Truchot (IMP, INSA Lyon) for their help with the composites preparation. The whole team benefited from the support of the IMP laboratory during the works at MATEIS, notably in terms of students relocation and access to experimental facilities. G.P.B., A.D., S.M. and J.B. thank the research direction of INSA-Lyon for financial support assigned to the project SUPERPONAI through the Bonus Qualité Recherche (BQR) internal program.

## **7. Authors Information**

L.R. and S.F. are both first authors of this manuscript. A.D. and G.P.B. are both corresponding authors of this manuscript.

## References

- [1] J. Currey, J. Taylor, The mechanical behaviour of some molluscan hard tissues., *J. Zool.* 173 (1974) 395–406. doi:10.1111/j.1469-7998.1974.tb04122.x.
- [2] J. Currey, Mechanical properties of mother of pearl in tension, *Proceedings of the Royal Society of London. Series B. Biological Sciences* 1125 (1977) 443–463. doi:10.1016/j.compscitech.2010.07.016.
- [3] H. Espinosa, J. Rim, F. Barthelat, M. Buehler, Merger of structure and material in nacre and bone—perspectives on de novo biomimetic materials, *Prog. Mater. Sci.* 54 (2009) 1059–1100. doi:10.1016/j.pmatsci.2009.05.001.
- [4] H.-L. Gao, S.-M. Chen, L.-B. Mao, Z.-Q. Song, H.-B. Yao, H. Colfen, X.-S. Luo, F. Zhang, Z. Pan, Y.-F. Meng, Y. Ni, S.-H. Yu, Mass production of bulk artificial nacre with excellent mechanical properties, *Nat. Commun.* 8 (2017) 287. doi:10.1038/s41467-017-00392-z.
- [5] G. Dwivedi, K. Flynn, M. Resnick, S. Sampath, A. Gouldstone, Bioinspired hybrid materials from spray-formed ceramic templates, *Adv. Mater.* 27 (2015) 3073–3078. doi:10.1002/adma.201500303.
- [6] T. Magrini, F. Bouville, A. Lauria, H. L. Ferrand, T. Niebel, A. Studart, Transparent and tough bulk composites inspired by nacre, *Nat. Commun.* 10 (2019) 2794. doi:10.1038/s41467-019-10829-2.
- [7] P. Hunger, A. Donius, U. Wegst, Platelets selfassemble into porous nacre during freeze casting, *J. Mech. Behav. Biomed. Mater.* 19 (2013) 87–93. doi:https://doi.org/10.1016/j.jmbbm.2012.10.013.
- [8] H. Saad, K. Radi, T. Douillard, D. Jauffres, C. Martin, S. Meille, S. Deville, A simple approach to bulk bioinspired tough ceramics, *Materialia* 12 (2020) 100807. doi:doi.org/10.1016/j.mtla.2020.100807.
- [9] J. Huang, W. Rubink, H. Lide, T. Scharf, R. Banerjee, M. Minary-Jolandan, Alumina–nickel composite processed via co-assembly using freeze-casting and spark plasma sintering., *Adv. Eng. Mater.* 21 (2019) 1801103. doi:10.1002/adem.201801103.
- [10] M. Garnier, D. Dunand, Ni–al<sub>2</sub>o<sub>3</sub> nacre-like composites through hot-pressing of freeze-cast foams, *Mater. Sci. Eng. A* 743 (2019) 190–196. doi:10.1016/j.msea.2018.11.033.

- [11] A. Wat, C. Ferraro, X. Deng, A. Sweet, A. Tomsia, E. Saiz, , R. Ritchie, Bioinspired nacre-like alumina with a metallic nickel compliant phase fabricated by spark-plasma sintering, *Small* 15 (2019) 1900573. doi:<https://doi.org/10.1002/sml.201900573>.
- [12] R. Henry, H. Saad, A. Doitrand, S. Deville, S. Meille, Interface failure in nacre-like alumina, *Journal of the European Ceramic Society* 40 (13) (2020) 4694–4699. doi:[10.1016/j.jeurceramsoc.2020.05.068](https://doi.org/10.1016/j.jeurceramsoc.2020.05.068).
- [13] S. Askarinejad, N. Rahbar, Mechanics of bioinspired lamellar structured ceramic/polymer composites: Experiments and models., *Int. J. Plast.* 107 (2018) 122–149. doi:[10.1016/j.ijplas.2018.04.001](https://doi.org/10.1016/j.ijplas.2018.04.001).
- [14] G. Du, A. Mao, J. Yu, J. Hou, N. Zhao, J. Han, Q. Zhao, W. Gao, T. Xie, H. Bai, Nacre-mimetic composite with intrinsic self-healing and shape-programming capability, *Nat. Commun.* 10 (2019) 1–8. doi:[10.1038/s41467-019-08643-x](https://doi.org/10.1038/s41467-019-08643-x).
- [15] T. Niebel, F. Bouville, D. Kokkinis, A. Studart, Role of the polymer phase in the mechanics of nacre-like composites, *Journal of the Mechanics and Physics of Solids* 96 (2016) 133–146. doi:<https://doi.org/10.1016/j.jmps.2016.06.011>.
- [16] Y. Wu, G. Cao, R. and Wu, W. Huang, Z. Chen, X. Yang, Y. Tu, From ultratough artificial nacre to elastomer: Poly(n-butyl acrylate) grafted graphene oxide nanocomposites, *Composites Part A: Applied Science and Manufacturing* 88 (2016) 156–164. doi:<https://doi.org/10.1016/j.compositesa.2016.05.028>.  
URL <https://www.sciencedirect.com/science/article/pii/S1359835X16301646>
- [17] T. Zhang, J. Sun, L. Ren, Y. Yao, M. Wang, X. Zeng, R. Sun, J. Xu, C. Wong, Nacre-inspired polymer composites with high thermal conductivity and enhanced mechanical strength, *Composites Part A: Applied Science and Manufacturing* 121 (2019) 92–99. doi:<https://doi.org/10.1016/j.compositesa.2019.03.017>.
- [18] B. Hu, W. Zhang, H. Guo, S. Xu, S. Li, M. Li, B. Li, Nacre-mimetic elastomer composites with synergistic alignments of boron nitride/graphene oxide towards high through-plane thermal conductivity, *Composites Part A: Applied Science and Manufacturing* 156 (2022) 106891. doi:<https://doi.org/10.1016/j.compositesa.2022.106891>.

- [19] S. N. G. Guner, A. F. Dericioglu, Nacre-mimetic epoxy matrix composites reinforced by two-dimensional glass reinforcements, *RSC Adv.* 6 (2016) 33184–33196. doi:10.1039/C5RA25049H. URL <http://dx.doi.org/10.1039/C5RA25049H>
- [20] S. Sapasakulvanit, X. Y. Chan, H. L. Ferrand, Fabrication and testing of bioinspired microstructured alumina composites with sacrificial interpenetrating polymer bonds, *Bioinspiration and Biomimetics* 18 (4) (2023) 046009. doi:10.1088/1748-3190/acd42d. URL <https://dx.doi.org/10.1088/1748-3190/acd42d>
- [21] F. Bouville, Strong and tough nacre-like aluminas: process-structure-performance relationships and position within the nacre-inspired composite landscape, *Journal of Material Research* (2019) 1–19doi:10.1557/jmr.2019.418.
- [22] F. Bouville, E. Maire, S. Meille, V. de Moortèle B, S. A.J., D. S., Strong, tough and stiff bioinspired ceramics from brittle constituents., *Nature Mater* 13 (2014) 508–514. doi:10.1038/nmat3915.
- [23] L. Mao, G. H. Gao, H. Yao, L. Liu, H. Colfen, G. Liu, S. Chen, S. Li, Y. Yan, Y. Liu, S. Yu, Synthetic nacre by predesigned matrix-directed mineralization, *Science* 354 (2016) 107–110. doi:10.1126/science.aaf899.
- [24] S. Valashani, F. Barthelat, A laser-engraved glass duplicating the structure, mechanics and performance of natural nacre, *Bioinspiration and Biomimetics* 10 (2015) 026005. doi:10.1088/1748-3190/10/2/026005.
- [25] R. Wilkerson, B. Gludovatz, J. Watts, A. Tomsia, G. Hilmas, , R. Ritchie, A novel approach to developing biomimetic (“nacre-like”) metal-compliant-phase (nickel–alumina) ceramics through coextrusion, *Advanced Materials* 28 (2016) 10061–10067. doi:<https://doi.org/10.1002/adma.201602471>.
- [26] E. Feilden, C. Ferraro, Q. Zhang, E. Garcia-Tunon, E. D’Elia, F. Giuliani, L. Vandeperr, E. Saiz, 3d printing bioinspired ceramic composites, *Scientific Reports* 7 (1) (2017) 13759. doi:10.1038/s41598-017-14236-9.
- [27] K. Evers, S. Falco, N. Grobert, R. Todd, Nacre-like alumina with unique high strain rate capabilities, *Journal of the European Ceramic Society* 40 (2020) 417–426. doi:10.1016/j.jeurceramsoc.2019.09.015.

- [28] L. Bonderer, A. Studart, L. Gauckler, Bioinspired design and assembly of platelet reinforced polymer films, *Science* 319 (5866) (2008) 1069–1073. doi:10.1126/science.1148726.
- [29] L. Bonderer, A. Studart, J. Woltersdorf, E. Pippel, L. Gauckler, Strong and ductile platelet-reinforced polymer films inspired by nature: microstructure and mechanical properties, *J Mater Res* 24 (9) (2009) 2741–2754. doi:10.1557/jmr.2009.0340.
- [30] Z. Tang, N. Kotov, S. Magonov, B. Ozturk, Nanostructured artificial nacre, *Nat Mater* 2 (6) (2003) 413–418. doi:10.1038/nmat906.
- [31] P. Podsiadlo, A. Kaushik, E. Arruda, A. Waas, B. Shim, J. Xu, Ultrastrong and stiff layered polymer nanocomposites, *Science* 318 (5847) (2007) 80–83. doi:10.1126/science.1143176.
- [32] S. Liff, N. Kumar, G. McKinley, High-performance elastomeric nanocomposites via solvent-exchange processing, *Nat Mater* 6 (1) (2007) 76–83. doi:10.1038/nmat1798.
- [33] E. Munch, M. Launey, D. Alsem, E. Saiz, A. Tomsia, R. Ritchie, Tough, bioinspired hybrid materials, *Science* 322 (5907) (2008) 1516–1520. doi:10.1126/science.1164865.
- [34] W. Woigk, E. Poloni, M. Grossman, F. Bouville, K. Masania, A. Studart, Nacre-like composites with superior specific damping performance, *Proceedings of the National Academy of Sciences* 119 (31) (2022) e2118868119. doi:10.1073/pnas.2118868119.
- [35] L. Bonderer, K. Feldman, L. Gauckler, Platelet-reinforced polymer matrix composites by combined gel-casting and hot-pressing. Part II: Thermoplastic polyurethane matrix composites, *Composites Science and Technology* 70 (13) (2010) 1966–1972. doi:10.1016/j.compscitech.2010.07.016. URL <https://www.sciencedirect.com/science/article/pii/S026635381000285X>
- [36] Z. Püspöki, M. Storath, D. Sage, M. Unser, Transforms and operators for directional bioimage analysis: A survey, in: W. H. De Vos, S. Munck, J.-P. Timmermans (Eds.), *Focus on Bio-Image Informatics*, Springer International Publishing, Cham, 2016, pp. 69–93. doi:10.1007/978-3-319-28549-8. URL <https://doi.org/10.1007/978-3-319-28549-8>
- [37] L. Bonderer, K. Feldman, L. Gauckler, Platelet-reinforced polymer matrix composites by combined gel-casting and hot-pressing. part i: Polypropylene matrix composites, *Composites Science and Technology* 70 (13) (2010) 1958–1965, iCCM-17: Composites In Biomedical Applications.

doi:10.1016/j.compscitech.2010.07.014.

URL <https://www.sciencedirect.com/science/article/pii/S0266353810002836>

- [38] A. Holt, P. Griffin, V. Bocharova, A. Agapov, A. Imel, M. Dadmun, J. Sangoro, A. Sokolov, Dynamics at the polymer/nanoparticle interface in poly (2-vinylpyridine)/silica nanocomposites, *Macromolecules* 47 (5) (2014) 1837–1843. doi:10.1021/ma5000317.
- [39] C. Fernández-de Alba, A. Jimenez, M. Abbasi, S. Kumar, K. Saalwächter, G. Baeza, On the immobilized polymer fraction in attractive nanocomposites: T<sub>g</sub> gradient versus interfacial layer, *Macromolecules* 54 (22) (2021) 10289–10299. doi:10.1021/acs.macromol.1c01135.
- [40] A. Papon, H. Montes, M. Hanafi, F. Lequeux, L. Guy, K. Saalwächter, Glass-transition temperature gradient in nanocomposites: evidence from nuclear magnetic resonance and differential scanning calorimetry, *Physical review letters* 108 (6) (2012) 065702.
- [41] P. Griffiths, G. Coativy, F. Dalmas, G. Falco, L. Jiang, Z. Xiang, M.-Q. Le, B. Ducharne, D. Le Roy, F. Méchin, J. Bernard, S. Meille, G. P. Baeza, Ultrafast remote healing of magneto-responsive thermoplastic elastomer-based nanocomposites, *Macromolecules* 55 (3) (2022) 831–843. arXiv:<https://doi.org/10.1021/acs.macromol.1c02046>, doi:10.1021/acs.macromol.1c02046. URL <https://doi.org/10.1021/acs.macromol.1c02046>
- [42] H. Landolt, R. Börnstein, *Thermodynamic Properties of Organic Compounds and Their Mixtures: Enthalpies of Fusion and Transition of Organic Compounds*. Subvol. A, Springer, 1995. doi:10.1007/b55145. URL <https://doi.org/10.1007/b55145>
- [43] H. Papananou, E. Perivolari, K. Chrissopoulou, S. H. Anastasiadis, Tuning polymer crystallinity via the appropriate selection of inorganic nanoadditives, *Polymer* 157 (2018) 111–121.
- [44] S. Sbrescia, J. Ju, T. Engels, E. Van Ruymbeke, M. Seitz, Morphological origins of temperature and rate dependent mechanical properties of model soft thermoplastic elastomers, *Journal of Polymer Science* 59 (6) (2021) 477–493. arXiv:<https://onlinelibrary.wiley.com/doi/pdf/10.1002/pol.20200791>, doi:<https://doi.org/10.1002/pol.20200791>. URL <https://onlinelibrary.wiley.com/doi/abs/10.1002/pol.20200791>

- [45] S. Sbrescia, J. Ju, C. Creton, T. Engels, M. Seitz, Effect of temperature, rate, and molecular weight on the failure behavior of soft block copoly(ether–ester) thermoplastic elastomers, *Soft Matter* 19 (2023) 5127–5141. doi:10.1039/D3SM00210A.  
URL <http://dx.doi.org/10.1039/D3SM00210A>
- [46] A. Mujtaba, M. Keller, S. Ilisch, H.-J. Radusch, T. Thurn-Albrecht, K. Saalwachter, M. Beiner, Mechanical properties and cross-link density of styrene–butadiene model composites containing fillers with bimodal particle size distribution, *Macromolecules* 45 (16) (2012) 6504–6515.
- [47] G. P. Baeza, J. Oberdisse, A. Alegria, K. Saalwächter, M. Couty, A.-C. Genix, Depercolation of aggregates upon polymer grafting in simplified industrial nanocomposites studied with dielectric spectroscopy, *Polymer* 73 (2015) 131–138.
- [48] Y. Yang, J. He, Q. Li, L. Gao, J. Hu, R. Zeng, J. Qin, S. X. Wang, Q. Wang, Self-healing of electrical damage in polymers using superparamagnetic nanoparticles, *Nature nanotechnology* 14 (2) (2019) 151–155.
- [49] A. E. Deatsch, B. A. Evans, Heating efficiency in magnetic nanoparticle hyperthermia, *Journal of Magnetism and Magnetic Materials* 354 (2014) 163–172.
- [50] L. Jiang, P. Griffiths, J. Balouet, T. Faure, R. Lyons, C.-A. Fustin, G. P. Baeza, Magneto-responsive nanocomposites with a metal–ligand supramolecular matrix, *Macromolecules* (2022).
- [51] N. Abando, H. Saad, M. Monclús, S. Deville, M.-A. J., J. Roa, Anisotropy effect of bioinspired ceramic/ceramic composites: Can the platelet orientation enhance the mechanical properties at micro- and submicrometric length scale?, *Journal of the European Ceramic Society* 41 (4) (2021) 2753–2762. doi:<https://doi.org/10.1016/j.jeurceramsoc.2020.12.039>.  
URL <https://www.sciencedirect.com/science/article/pii/S0955221920310086>
- [52] X. Chan, C. Chua, S. Tan, H. Le Ferrand, Energy dissipation in composites with hybrid nacre-like helicoidal microstructures, *Composites Part B: Engineering* 232 (2022) 109608. doi:<https://doi.org/10.1016/j.compositesb.2021.109608>.  
URL <https://www.sciencedirect.com/science/article/pii/S1359836821009732>
- [53] S. Akurati, A. Jansson, J. Jones, D. Ghosh, Deformation mechanisms in ice-templated alumina–epoxy composites for the different directions of uniaxial compressive loading, *Materialia* 16

(2021) 101054. doi:<https://doi.org/10.1016/j.mtla.2021.101054>.

URL <https://www.sciencedirect.com/science/article/pii/S2589152921000570>

[54] T. Duminy, R. Henry, J. Adrien, A. Doitrand, S. Meille, Anisotropic fracture in nacre-like alumina, *Theoretical and Applied Fracture Mechanics* 123 (2023) 103710. doi:<https://doi.org/10.1016/j.tafmec.2022.103710>.

URL <https://www.sciencedirect.com/science/article/pii/S0167844222004591>